Photocatalytic Oxidation of Rhodamine 6G Dye Using Magnetic TiO_2@Fe_3O_4/FeZSM-5

M. Dükkancı*
Ege University,
Chemical Engineering Department,
35100, Bornova/İzmir/Turkey

doi: https://doi.org/10.15255/CABEQ.2020.1909
Original scientific paper
Received: December 27, 2020
Accepted: March 16, 2021

Efficient decolorization of Rhodamine 6G dye (Rh 6G) using magnetic TiO_2@Fe_3O_4/FeZSM-5 photocatalyst was carried out in a batch reactor equipped with two visible lights (high-pressure Na lamps). The photocatalyst was synthesized and characterized by X-ray diffraction, scanning electron microscopy, energy dispersive X-ray spectroscopy, diffuse reflectance spectroscopy and vibrating sample magnetometry. The effects of initial Rh 6G concentration, catalyst loading, and pH were investigated on photocatalytic oxidation of Rh 6G. Maximum decolorization of 98.2 % was found at optimum conditions of 20 ppm Rh 6G, 1 g L^{-1} of catalyst, and pH of 13.04. Central composite design was used for the optimization of photocatalytic degradation of Rh 6G. Predicted decolorization efficiencies were found to be in good agreement with experimental values with high regression coefficient of 98.8 %. In addition to color removal, the toxicity of the Rh 6G aqueous solution was significantly reduced after photocatalytic oxidation. Small reduction of activity (from 34.6 % to 30.5 %) showed the stability of the catalyst after three consecutive runs. Due to the magnetic property of the catalyst, it could be removed from the solution with the help of external magnetic field. This prevents the loss of catalyst and reduces the extra separation cost, which is desired in industrial or large-scale applications.

Keywords:
magnetic photocatalyst, photocatalytic oxidation, Rhodamine 6G, TiO_2@Fe_3O_4/FeZSM-5, toxicity

Introduction

Water is an indispensable source of life for all living things. However, population growth, industrial growth, development of urban life, and unconscious use of water reduce the natural water resources day by day and increase the need for water treatment systems (drinking water and utility water). The treatment of toxic pollutants from wastewater or drinking water, and the use of systems in which water is recycled is a matter of conscious societies. Petroleum refinery, textile industry, sewage, domestic, hospital, and agricultural wastewaters all contain toxic pollutants.[1] Among them, wastewater coming from various textile industries is an important source of environmental pollution due it containing an excessive amount of different toxic dyes. It is estimated that nearly 18–20 % of the total production of dyes is discharged into the environment throughout the textile dyeing process.[2] The chemical oxygen demand (COD) in water effluent increases due to the presence of organic dyes, which may also exhibit high toxicity, carcinogenicity, and mutagenicity. Rhodamine 6G (Rh 6G) dye, used mostly as a colorant in the textile industries, is among the most toxic dyes. It is a non-volatile compound, highly water soluble, and dark reddish orange in color.[2,3]

Due to the aforementioned reasons, it is very important to treat wastewater coming from textile industry with proper treatment method. Dye removal technologies can be divided into three categories: biological, chemical, and physical. Biological treatment has low cost, but is ineffective for treatment of wastewater containing non-biodegradable dyes. Flocculation, filtration or coagulation as physical processes are economically feasible but they produce high amounts of sludge. Ion exchange technology has high capacity for some dyes, but in some cases it is not cost effective. Adsorption is another option that has low costs of preparation and usage.[4] Gao and coworkers[5] investigated the adsorption of Methyl Orange dye on mesoporous Fe_3O_4-SiO_2-TiO_2 photocatalyst, which can be separated easily from the solution by magnet. They observed about 95 % adsorption of Methyl Orange. Babaei *et al.*[6] used oak wood as an agrowaste, which was activated to

*Corresponding author: E-mail: meral.dukkanci@ege.edu.tr,
Tel: 902323112288

prepare biochar and used as an effective biosorbent to remove Methylene Blue dye from aqueous solution. Kermani *et al.*[7] studied the adsorption of Reactive Red 198 and Reactive Blue 29 on powder and ash from *Rosa damascena* waste. In the study by Azari *et al.*,[8] adsorption of Basic Violet 16 was evaluated on magnetic zero-valent iron-activated carbon nanocomposite. They observed that, in optimal conditions, magnetic zero-valent iron-activated carbon nanocomposite had the potential to remove Violet 16 dyes. In recent years, advanced oxidation processes (AOPs) have been focused on the treatment of non-biodegradable organic dyes. AOPs are performed under ambient conditions without requiring high temperature and pressure; they are based on the production of highly reactive radicals (·OH, O_2^{-}). The resulting radicals oxidize the organic pollutants and convert them into CO_2 and water. In the present study, photocatalytic oxidation was used as one of the AOPs that uses light energy to activate semiconductor photocatalyst. TiO_2 is the best known photocatalyst because it is chemically stable, non-toxic, has good oxidizing strength, and usage cost.[9] However, the disadvantage of using TiO_2 in practical applications is the difficulties in separation from solution and recovery. To sort out this problem, TiO_2 particles can be coated on magnetic cores such as Fe_3O_4, and the coated particles can be collected by the action of an external magnetic field. In addition, immobilization of TiO_2 on supporting materials such as zeolite or clay can improve the separation efficiency, and increase specific surface area where the catalytic reactions occur.[10,11] However, TiO_2 catalysts can be activated under UV light irradiation (below 385 nm) due to a wide band gap energy of 3.0–3.2 eV.[12] However, ultraviolet light is only 4–5 % and visible light is approximately 40 % of the sun spectrum. Therefore, significant efforts have been made in recent years to develop TiO_2-based photocatalysts that can use visible light in solar radiation or artificial light efficiently. Beside magnetic property of Fe_3O_4, it also shifts the catalytic activity of TiO_2 towards the visible light region and prevents the recombination of electron-hole pairs. In this concept, Babaei and coworkers[13] studied the degradation of 4-chlorophenol using a photocatalytic sulfate radical-based AOP by ferroferric oxide nanoparticles anchored on activated carbon. They achieved 99 % 4-chlorophenol removal and 49 % TOC removal at optimum operating conditions. TiO_2 decorated on ferroferric oxides coupled with activated carbon was used as a magnetic heterogeneous catalyst in peroxydisulfate activated photocatalytic oxidation of tetracycline.[14] After 15 min of reaction, 96 % tetracycline and 72.1 % TOC removals were obtained at optimum operating conditions: pH: 5, catalyst: 0.3 g L^{-1}, PS: 1 mM. In the study by Bashiri *et al.*,[15] TiO_2 decorated magnetic reduced graphene oxide was fabricated by hydrothermal method, and its activity was tested on metronidazole photocatalytic oxidation. Almost complete degradation and 39 % TOC removal was achieved within 120 min of reaction.

There are several studies in literature that studied the activity of Fe_3O_4/TiO_2,[11,12,16–20] or Fe_3O_4/TiO_2 supported on carbon-based materials,[21–25] CuO,[26] SiO_2,[9,27,28] and bentonite.[29] However, to our knowledge, no study has so far investigated the activity of the TiO_2 supported Fe_3O_4/zeolite (TiO_2@Fe_3O_4/FeZSM-5) magnetically separable composite catalyst. In this frame, the main target of this study was the development and characterization of magnetically separable TiO_2@Fe_3O_4/FeZSM-5 photocatalyst to be used for the decolorization of Rh 6G dye under visible light irradiation. The effects of catalyst loading, initial pH, and initial dye concentration on decolorization were investigated using Central Composite Design (CCD) methodology. In addition, it was thought that examining not only the photocatalytic activity of the synthesized catalyst, but also the reduction on the toxicity effect of Rh 6G wastewater would make positive contributions to the relevant literature.

Experimental

Materials

The dye, Rhodamine 6G, was obtained from Sigma-Aldrich (Molecular formula = $C_{28}H_{31}N_2O_3Cl$, M_w = 479.01 g mol^{-1}, λ_{max} = 526 nm). Iron containing ZSM-5 zeolite (FeZSM-5) was obtained from Clariant-Süd-Chemie with a trade number of Fe-TZP302. TiO_2 (P-25) was obtained from Sigma-Aldrich. H_2O_2 solution (35 wt.%) of analytical grade was purchased from Merck. All aqueous solutions were prepared with distilled water obtained from a Millipore Direct Q3 purification unit.

Catalyst preparation

Preparation of Fe_3O_4 catalyst

Fe_3O_4 magnetic nanoparticles were prepared as follows: Firstly, $FeCl_2{\cdot}4H_2O$ (1.0 g) and $FeCl_3{\cdot}6H_2O$ (2.6 g) mixture (molar ratio of 1:2) was dissolved in 2.5 mL of HCl (2 M) solution. An amount of 50 mL of 25 % v/v ammonia aqueous solution was then added into above solution under continuous stirring at room temperature with bubbling nitrogen gas. The Fe_3O_4 precipitate was produced immediately by adding aqueous ammonia. This precipitate was filtered, washed up to pH=8 with deionized water, and oven-dried at 60 °C for 3 h.[11,30]

Preparation of TiO_2@Fe_3O_4/FeZSM-5 zeolite catalyst

In the preparation of TiO_2@Fe_3O_4/FeZSM-5, firstly 1.0 g of FeZSM-5 zeolite powder was put in aqueous solution (200 mL) containing 5.0 g of $FeCl_3 \cdot 6H_2O$ and 2.5 g of $FeSO_4 \cdot 7H_2O$ under nitrogen bubbling at 343 K. Thereupon, 10 mL of 8 mol L^{-1} aqueous NaOH solution was prepared, and then dropped slowly into above solution in order to adjust the pH to 11, and the mixture was stirred continuously for 1 h. The mixture was heated in an oven under air atmosphere at 343 K for 4 h. The particles were then washed with distilled water until neutral pH and oven-dried at 373 K for 3 h to obtain Fe_3O_4/FeZSM-5 zeolite.

The prepared Fe_3O_4/FeZSM-5 zeolite (2.5 g) was put in ethanol (80 mL). The mixture was sonicated for 20 min in an ultrasonic bath (C.E.I.A model 102 digit, Italy) at a frequency of 40 kHz, and at a power of 84 W. Thereafter, tetrabutyl titanate (20 mL) as titanium source was added to the mixture and stirred with mechanical stirrer, and sonicated for another 20 min. An amount of 80 mL of ethanol and aqueous nitric acid (1 mL 10 M HNO_3 + 16 mL distilled water) were then added to form a colloidal solution. The mixture was stirred for 30 min and allowed to stand for one day. Finally, the mixture was dried at 353 K and calcined at 773 K for 3 h to produce TiO_2@Fe_3O_4/FeZSM-5 magnetically separable composite photocatalyst.[29,30]

Catalyst characterization

Scanning electron microscopy (QUANTA 400F Field Emission SEM) was used to determine morphological properties of the catalysts. To determine surface area and average pore diameter of as-prepared samples, nitrogen adsorption and desorption isotherms were measured at 77 K using Micromeritics Gemini V apparatus. The magnetic properties of the Fe_3O_4 and TiO_2@Fe_3O_4/FeZSM-5 composite were measured using vibration sample magnetometer (Cryogenic Limited PPMS). Crystalline structure of the samples was determined using the powder X-ray diffraction (XRD) analysis in the range of 10-80° with a Philips X'Pert Pro apparatus with Cu-Kα radiation. UV–Vis diffuse reflectance spectroscopy (DRS) was used to measure band gap energy of TiO_2@Fe_3O_4/FeZSM-5 sample by UV-Vis DRS/Shimadzu 2600 with ISR integrating sphere attachment that holds the solid powder catalyst sample.

Photocatalytic experiments

The photocatalytic activity of the prepared sample was evaluated by the decolorization of Rh 6G. Typically, catalyst (0.25–0.75 mg) was dispersed in 0.5 dm^3 of Rh 6G aqueous solution. Before the light irradiation, the suspension was stirred in the dark for 30 min to establish the adsorption-desorption equilibrium of the Rh 6G on the catalyst surface. H_2O_2 was then added as oxidant, and the visible light lamps were turned on. A cooling water-jacketed batch reactor was used. Two visible light lamps (high-pressure Na lamps, each 150 W) were used as light source placed at two outer sides of reactors. The photocatalytic process for the degradation of Rh 6G took 5 h. The reaction temperature was kept constant at 298±1 K by circulating cooling water through the reactor jacket. The glass reactor was housed in a sealed box to avoid photochemical reactions influenced by natural light. Samples were taken periodically and put into the iced-bed to stop the reaction, centrifuged for 5 min, and then analyzed with UV spectrophotometer (Genesys 10S UV-vis) at 526 nm. Parametric studies were performed over TiO_2@Fe_3O_4/FeZSM-5 photocatalyst and the effects of initial Rh 6G concentrations, pH of the solution, and catalyst loading were studied on decolorization of Rh 6G. The response surface methodology (RSM) was used in the CCD of experiments with three factors, three levels, and one response variable, the decolorization of Rh 6G as given in Tables 2 and 3.

Results and discussion

Characterization of prepared catalysts

Morphology of prepared Fe_3O_4 and TiO_2@Fe_3O_4/FeZSM-5 catalysts was discussed in the previous study.[30] SEM images showed that particles had agglomerated and were randomly distributed. The atomic compositions of Fe_3O_4 and TiO_2@Fe_3O_4/FeZSM-5 composite were determined by SEM-EDX. The elements of Fe, Ti and O, and Na, Si and Al (in the case of TiO_2@Fe_3O_4/FeZSM-5, Fig. 1) were observed in the composites.[30] As known, ZSM-5 zeolite (structure type of MFI) is an aluminosilicate zeolite mineral belonging to the pentasil family of zeolites. Its chemical formula can be written as $Na_nAl_nSi_{96-n}O_{192} \cdot 16H_2O$ ($0<n<27$).[31] Thus, according to SEM-EDX results, in addition to Fe, Ti and O elements, the presence of Na, Al and Si in the TiO_2@Fe_3O_4/FeZSM-5 (Fig. 1b) provides the composite structure of Fe_3O_4 + TiO_2 + ZSM-5 zeolite.

The magnetization–hysteresis curves suggest that bare Fe_3O_4, and TiO_2@Fe_3O_4/FeZSM-5 particles show ferromagnetic and superparamagnetic behavior with magnetization saturation value of 21.7, and 9.13 emu g^{-1}, respectively. The figure is given in Supplementary Material (Fig. 1S). The reduction of saturation magnetization is related with the existence of nonmagnetic TiO_2 shells on the surface of magnetic Fe_3O_4. Due to their magnetic properties,

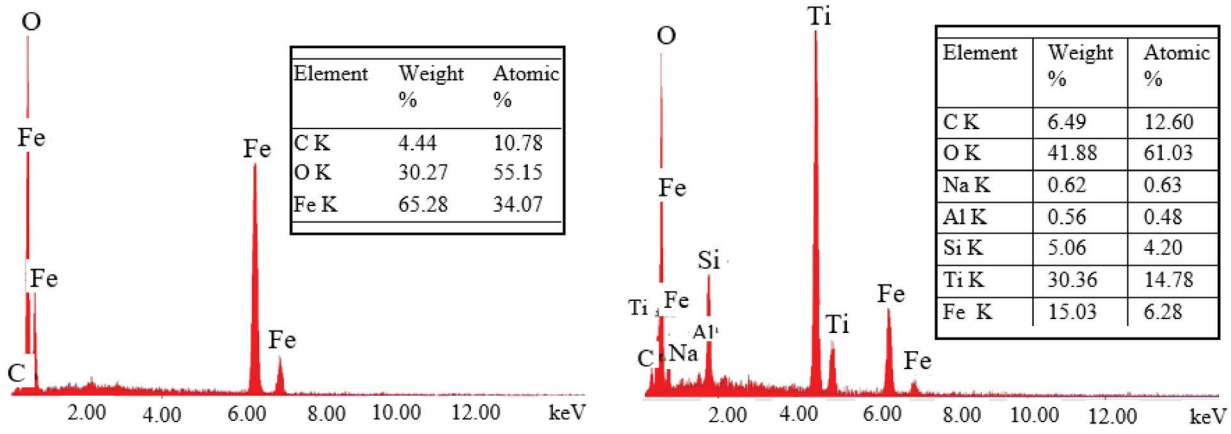

Fig. 1 – *SEM-EDX results of a) Fe_3O_4 b) TiO_2@Fe_3O_4/FeZSM-5 composite*

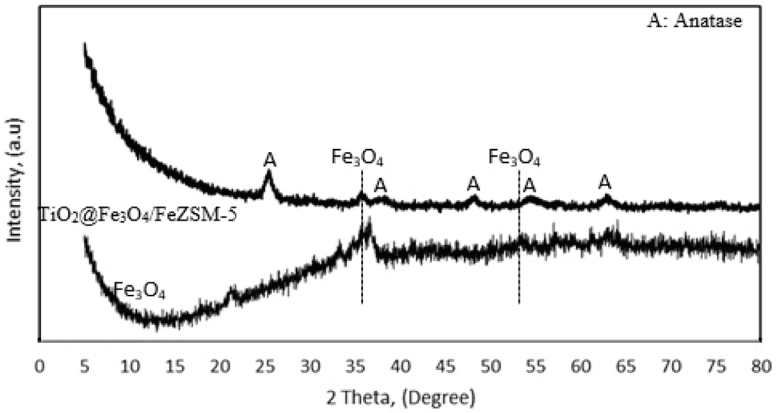

Fig. 2 – *XRD analysis of Fe_3O_4 and TiO_2@Fe_3O_4/FeZSM-5 particles*

catalysts were recollected using external magnet (image shown as inset), which generally reduces the separation cost after the photocatalytic reaction in practical applications.[30]

XRD diffractograms of prepared catalysts are given in Fig. 2. All the diffraction peaks at 2θ = 25.4°, 37.9°, 48.1°, 55.1° and 62.8° of TiO_2 can be indexed to the anatase phase of TiO_2. The diffraction peaks at around 35.4° and 53.4° could be assigned to the diffraction of Fe_3O_4. Although the typical diffractions of the MFI framework (2θ = 7–9°, 23–25°) could not be observed in XRD diffractograms, the presence of aluminosilicate structure was confirmed by SEM-EDX analysis. This may be due to the complete coverage of surface of FeZSM-5 zeolite with TiO_2 and Fe_3O_4.

The BET-surface area (S_{BET}), total pore volume (V_p), maximum volume adsorbed, and average pore diameter based on BJH method were all obtained from nitrogen adsorption/desorption measurements, and presented in Table 1.

As may be seen in Table 1, TiO_2@Fe_3O_4/FeZSM-5 has a mesoporous (d_{ave} = 5.59 nm) structure with high surface area of 105.83 $m^2\ g^{-1}$.

Table 1 – *Nitrogen adsorption results of prepared catalysts*

Catalyst	BET surface area, $m^2\ g^{-1}$	Total pore volume, $cm^3\ g^{-1}$	Max. volume adsorbed, $cm^3\ g^{-1}$	Average pore diameter, d_{ave} (4V/A by BJH), nm
Fe_3O_4	77.07	0.26145	169.03	10.7
TiO_2@Fe_3O_4/FeZSM-5	105.83	0.161885	104.66	5.59

The UV–Vis DRS spectrum of the TiO_2@Fe_3O_4/FeZSM-5 photocatalyst is given in Fig. 3. The band gap energy of the catalyst was obtained from the plots of the Kubelka-Munk function given in Eq. 1:

$$\left(F(R)\cdot hv\right)^{1/n} = B\left(hv - E_g\right) \quad (1)$$

where h is Planck's constant, v is the light frequency, B is a constant, $F(R) = (1–R)^2/2R$, R is reflectance, and $hv = (1240/\lambda)$ eV. For an indirect transition, n is taken as 2, whereas for a direct transition,

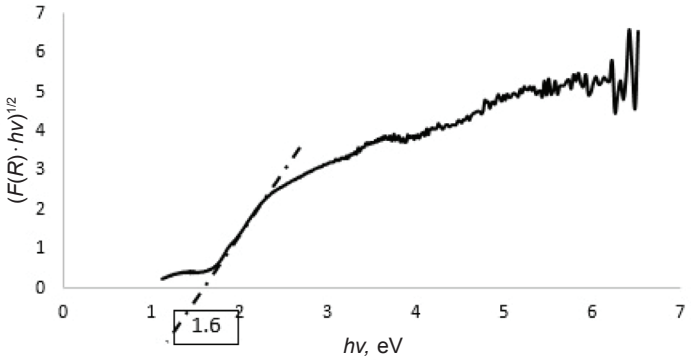

Fig. 3 – *UV-Vis DRS analysis of TiO_2@Fe_3O_4/FeZSM-5*

n is taken as 0.5. It has been suggested that anatase TiO_2 follows an indirect transition,[32,33] and thus $n = 2$ was used in this study. According to Fig. 3, the band gap energy value of TiO_2@Fe_3O_4/FeZSM-5 photocatalyst was 1.6 eV, which was much smaller than anatase TiO_2 of 3.2 eV. However, conduction band energy level (E_{CB}) and valence band energy level (E_{VB}) should also be known to explain charge mobility in photocatalytic oxidation. To achieve visible light degradation of pollutants, conduction band minimum of photocatalyst should be more negative than the $O_2/O\bullet_2^-$ reduction potential to produce $O\bullet_2^-$. Similarly, valence band maximum of photocatalyst should be more positive than the oxidation potential of $OH^-/\bullet OH$ and $H_2O/\bullet OH$ to produce hydroxyl radicals. Both •OH and $O\bullet_2^-$ are free radicals with high oxidizing potential. Therefore, in addition to narrowing the band gap of semiconductor, the E_{CB} and E_{VB} values should also meet the redox capacity for efficient photocatalytic oxidation.[34]

Decolorization of Rh 6G over TiO_2@Fe_3O_4/FeZSM-5 photocatalyst

In decolorization of Rh 6G, blank experiments were performed firstly at the following conditions: $T = 298$ K, 10 mM H_2O_2, 1 g L^{-1} catalyst, 20 mg L^{-1} initial concentration of Rh 6G, initial dye pH of ~8.0. Fig. 4 shows the results.

As seen in Fig. 4, H_2O_2 was activated slightly with visible light. There was no decolorization when H_2O_2 was used alone, while 8.18 % of decolorization was achieved in the presence of visible light. Photocatalytic activity of Fe_3O_4 was 10.2 % at the end of 300 min of reaction time; however, 34.6 % of decolorization was achieved after the same reaction time in the presence of TiO_2@Fe_3O_4/FeZSM-5 photocatalyst.

After blank experiments, parametric studies were performed over TiO_2@Fe_3O_4/FeZSM-5 photocatalyst to achieve higher photo-decolorization. The effects of initial Rh 6G concentration, pH of the solution and catalyst loading as parameters were studied. The RSM was used in the CCD of experiments to develop mathematical correlation between the parameters and decolorization of Rh 6G. In other words, the experiments were designed using CCD with three factors at three levels and one response variable, the decolorization of Rh 6G.

The data were fitted to the second-order polynomial model, Eq. 2:

$$Y = \beta_0 + \sum \beta_i X_i + \sum \beta_{ii} X_i^2 + \sum \beta_{ij} X_i X_j \quad (2)$$

where, Y is the predicted response, β_0 is the value of the fitted responses at the central point of the experiment (offset term), β_i, β_{ii}, β_{ij} are the linear, squared, and interaction-regression coefficients of the model, respectively. X_i and X_j are the coded variables.

Initial Rh 6G concentration, catalyst loading, and pH are displayed as X_1, X_2 and X_3, respectively, in the model equation. Other factors, such as stirring speed of 500 rpm, temperature of 298 K, and H_2O_2 amount of 10 mM were held constant. The low, middle, and high levels of each variable were designed as –1.681, 0, and +1.681, respectively. The independent variables and their levels are listed in Table 2.

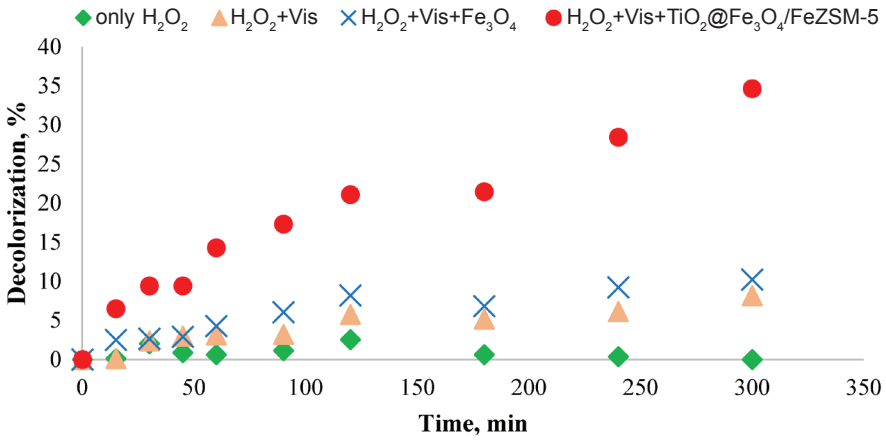

Fig. 4 – *Blank experiments for decolorization of Rh 6G*

Table 2 – *Independent variables and their levels in photocatalytic oxidation of Rh 6G*

Variables						
Un-coded	Coded	Levels				
		–1.681	–1	0	1	1.681
Initial concentration, mg L^{-1}	X_1	3.18	10	20	30	36.81
Catalyst loading, g/500 mL	X_2	0.079	0.25	0.5	0.75	0.92
pH	X_3	2.95	5	8	11	13.04

Table 3 – *Central composite design of the photocatalytic oxidation of Rh 6G for three independent variables*

Runs	X_1	X_2	X_3	Initial concentration, mg L^{-1}	Catalyst loading, g/500 mL	pH	Decolorization, %
1	1.681	0	0	36.81	0.5	8.00	34.2
2	0	0	0	20	0.5	8.00	31.8
3	–1.68	0	0	3.18	0.5	8.00	57.8
4	**0**	**0**	**1.681**	**20**	**0.5**	**13.04**	**98.2**
5	–1	–1	1	10	0.25	11.00	80.6
6	1	–1	1	30	0.25	11.00	52.6
7	0	0	0	20	0.5	8.00	36.8
8	0	0	0	20	0.5	8.00	34.8
9	0	0	0	20	0.5	8.00	30.2
10	1	1	1	30	0.75	11.00	94.8
11	1	–1	–1	30	0.25	5.00	0
12	0	1.681	0	20	0.92	8.00	55.0
13	–1	1	–1	10	0.75	5.00	28.5
14	1	1	–1	30	0.75	5.00	29.1
15	0	0	0	20	0.5	8.00	33.8
16	0	0	–1.681	20	0.5	2.95	16.1
17	0	0	0	20	0.5	8.00	30.4
18	–1	–1	–1	10	0.25	5.00	32.9
19	–1	1	1	10	0.75	11.00	83.5
20	0	–1.681	0	20	0.079	8.00	12.9

The experimental values of Rh 6G decolorization under various experimental conditions are given in Table 3. The significance of the parameters on the photocatalytic oxidation of Rh 6G was determined using Analysis of Variance (ANOVA) with a confidence level of 95 % (Minitab-19 software, Academic version).

By analyzing the experimental results through CCD, an empirical correlation for the best photodegradation was found to be:

$$Y = 108.2 - 5.151X_1 - 77.1X_2 - 10.85X_3 + 0.0541X_1 \cdot X_1 + 18.3X_2 \cdot X_2 + 1.039X_3 \cdot X_3 + \\ + 3.640X_1 \cdot X_2 + 0.0650X_1 \cdot X_3 + 3.40X_2 \cdot X_3$$

where X_1 is the initial concentration of Rh 6G (mg L^{-1}), X_2 is the catalyst loading (g/500 mL), X_3 is the pH, and Y is the decolorization, %.

Table 4 – *ANOVA of the response for decolorization of Rh 6G*

Term	Degrees of freedom	Sum of squares	Mean square	F value	P value
Initial concentration, X_1	1	576	575.97	34.15	$1.63 \cdot 10^{-4}$
Catalyst loading, X_2	1	1447.6	1447.58	85.82	$3.19 \cdot 10^{-6}$
pH, X_3	1	9441.0	9441.05	559.69	$4.10 \cdot 10^{-10}$
X_1^2	1	421	421.03	24.96	$5.41 \cdot 10^{-4}$
X_2^2	1	18.9	18.89	1.12	$3.15 \cdot 10^{-1}$
X_3^2	1	1259.1	1259.13	74.64	$5.97 \cdot 10^{-6}$
X_1X_2	1	662.5	662.48	39.27	$9.29 \cdot 10^{-5}$
X_1X_3	1	30.4	30.42	1.80	$2.09 \cdot 10^{-1}$
X_2X_3	1	52.0	52.02	3.08	$1.09 \cdot 10^{-1}$
Error	10	168.7	16.87		
Lack of fit	5	134.3	26.87	3.91	$8.04 \cdot 10^{-2}$
Pure error	5	34.4	6.87		
Total	19	13929.6			
R^2		0.9879			
R^2 – adjusted		0.9770			
R^2 – predicted		0.9229			

Table 4 shows the ANOVA results. The significance of main and interaction effect of each independent parameter was evaluated based on F-values and P-values. The larger magnitude of F-value supports the more significant effect of each independent variable on model response. The P-values less than 0.05 indicate that parameter had a significant effect on the response, while the lack-of-fit of model is not significant.[35,36]

According to ANOVA analysis, high R^2 value of 0.9879 and high lack of fit ($P > 0.05$) of 0.08 show that the model was well-fitted to experimental data. As seen in Table 4, all the investigated parameters had a significant effect on decolorization of Rh 6G. Fig. 5 shows the interaction plot for decolorization of Rh 6G.

Fig. 6 shows the surface plot of decolorization % vs catalyst loading, initial concentration at pH = 8 (a), surface plot of decolorization % vs pH, initial concentration at the constant catalyst loading of 0.5 g/500 mL (b), and surface plot of decolorization % vs pH, catalyst loading at the constant initial concentration of Rh 6G of 20 mg L^{-1} (c).

As seen in Figs. 5 and 6, increasing initial concentration of Rh 6G decreased the decolorization degree. This may be explained by the competition of Rh 6G molecules and the formed intermediates for active radicals of ·OH and/or O_2^{-}. Another reason for the reduction in color removal may be the capability of Rh 6G molecules to reflect light and thus prevent it from reaching the catalyst surface. The decrease in decolorization was more drastic in the lowest catalyst loading used in this study (0.25 mg/500 mL). Increasing catalyst loading enhances the number of active sites available on the catalyst support, thus the number of active radicals (·OH, O_2^{-}·) responsible for the photocatalytic oxidation increases. This has a positive impact on the decolorization degree, and the decolorization degree of Rh 6G increased with increased catalyst loading at all studied pH values. The effect of pH played the most significant role in photocatalytic oxidation of Rh 6G (with P value of $4.1 \cdot 10^{-10}$, Table 4). It was clear that alkaline pH was favorable for decolorization of Rh 6G, because at pH values higher than the zero point charge (zpc) of titania (6.25),[37] the surface became negatively charged. Rh 6G is a cationic dye with hydrophobic character under basic conditions (at higher pH than its pK_a value of 6.13) as the free electron pair on the amine nitrogen (primary amine group) transfers charges from amine nitrogen to aromatic rings. Due to the electrostatic interaction between Rh 6G cations of Rh 6G and negatively charged catalyst surface, more Rh 6G could adsorb on the catalyst surface for photocatalytic oxidation. Rh 6G molecule becomes hydrophilic in nature under acidic pH due to the protonation of nitrogen in the secondary amine group of the xanthene ring (pH < pK_a), which hinders the adsorption of Rh 6G on the catalyst surface, and thus has a negative effect on the photocatalytic decolorization.[35,36,38–40]

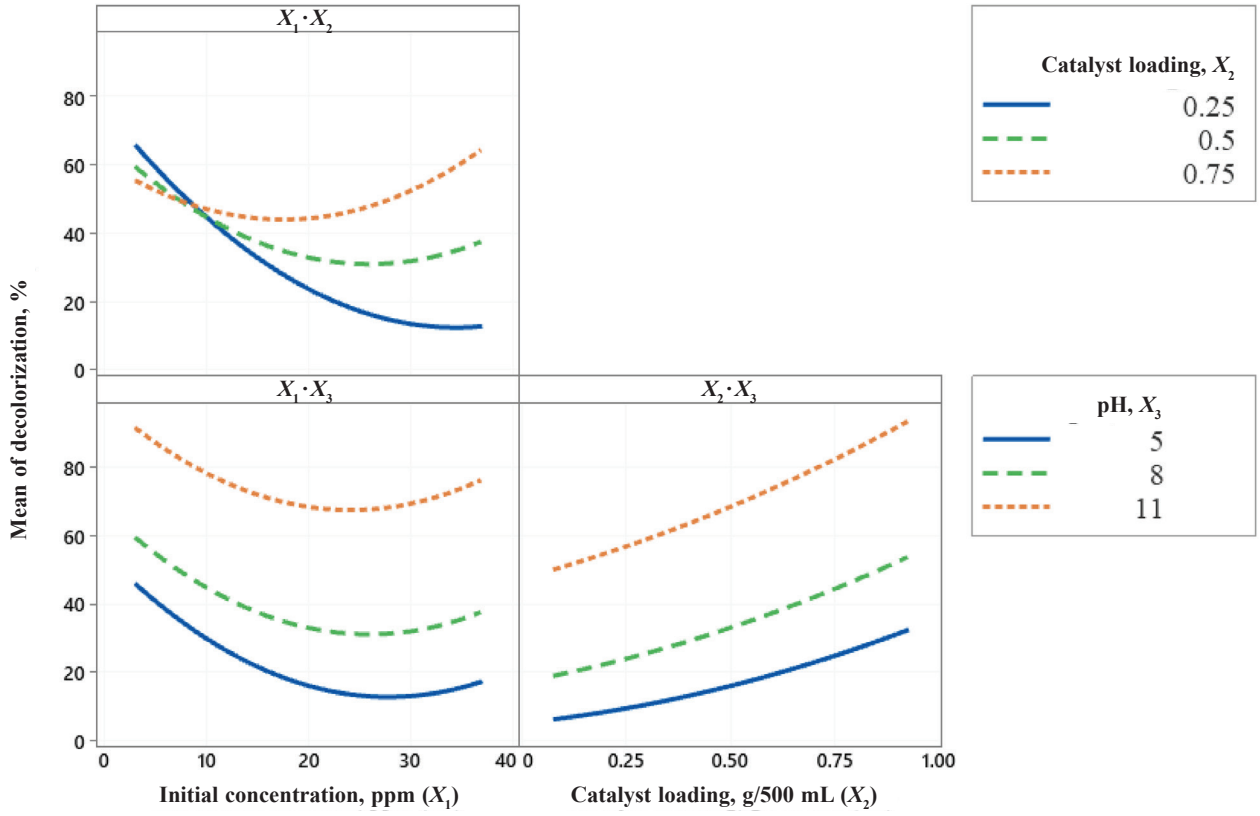

Fig. 5 – *Interaction plot for decolorization %*

Main effect plot of decolorization of Rh 6G is given in Fig. 2S in Supplementary Material. Higher decolorization of Rh 6G was achieved at low initial concentration, with high catalyst loading and at alkaline condition. The higher positive effect of pH than that of initial concentration and catalyst loading can be seen clearly.

Maximum photocatalytic decolorization percentage of 98.2 % was found at optimum conditions set as follows: 20 ppm Rh 6G, 1 g L^{-1} of catalyst, and basic pH of 13.04. At these conditions, the measured TOC removal was 40 % within the same reaction time of 300 min.

Fig. 7 presents the experimental (actual) and predicted values for decolorization of Rh 6G. The high correlation (R^2 = 98.8 %) between the experimental data and predicted values showed that the experimental data fitted well with the model in the range studied.

Stability and reusability of the TiO_2@Fe_3O_4/FeZSM-5 photocatalyst

Stability of the catalyst was tested in photocatalytic oxidation of Rh 6G over TiO_2@Fe_3O_4/FeZSM-5 photocatalyst in terms of reusability. The catalyst was separated easily after each run by external magnet, washed thoroughly with pure water and ethanol, dried at 80 °C for 3 h, and then calcined at 500 °C for 3 h. The calcined catalyst was reused for the next run. Fig. 8 shows the decolorization of Rh 6G after 3 consecutive runs. About 34.6 %, 32.6 %, and 30.5 % of Rh 6G dye removal was obtained after 5 h in the first, second, and third run, respectively. As seen in Fig. 8, decolorization of Rh 6G had decreased slightly after three consecutive runs that deduce the stability and reusability of the catalyst.

Toxicity measurements

Toxicity measurements were conducted with 20 mg L^{-1} of untreated Rh 6G and treated Rh 6G after photocatalytic oxidation at the following conditions: T = 298 K, 10 mM H_2O_2, 0.5 g/500 mL catalyst, 150+150 W UV–Vis lamps, initial dye pH of 8.

Experiment was done according to the modified method given by Arambasic *et al.*,[41] Demir *et al.*[42] and Dükkancı.[43] *Lepidium sativum* L. (Garden cress) seeds were used to evaluate the toxicity of 20 mg L^{-1} Rh 6G solution before and after 300 min of photocatalytic treatment. For this purpose, filter paper was placed in a 9-cm glass Petri dish. Twenty-five seeds of cress were then placed on filter paper homogeneously, and the filter paper was moistened with 5 mL of the test solution. Closed Petri dishes were placed in the dark for 120 hours at room temperature. At the end of 120 hours, the root lengths of the seeds were measured for the distilled

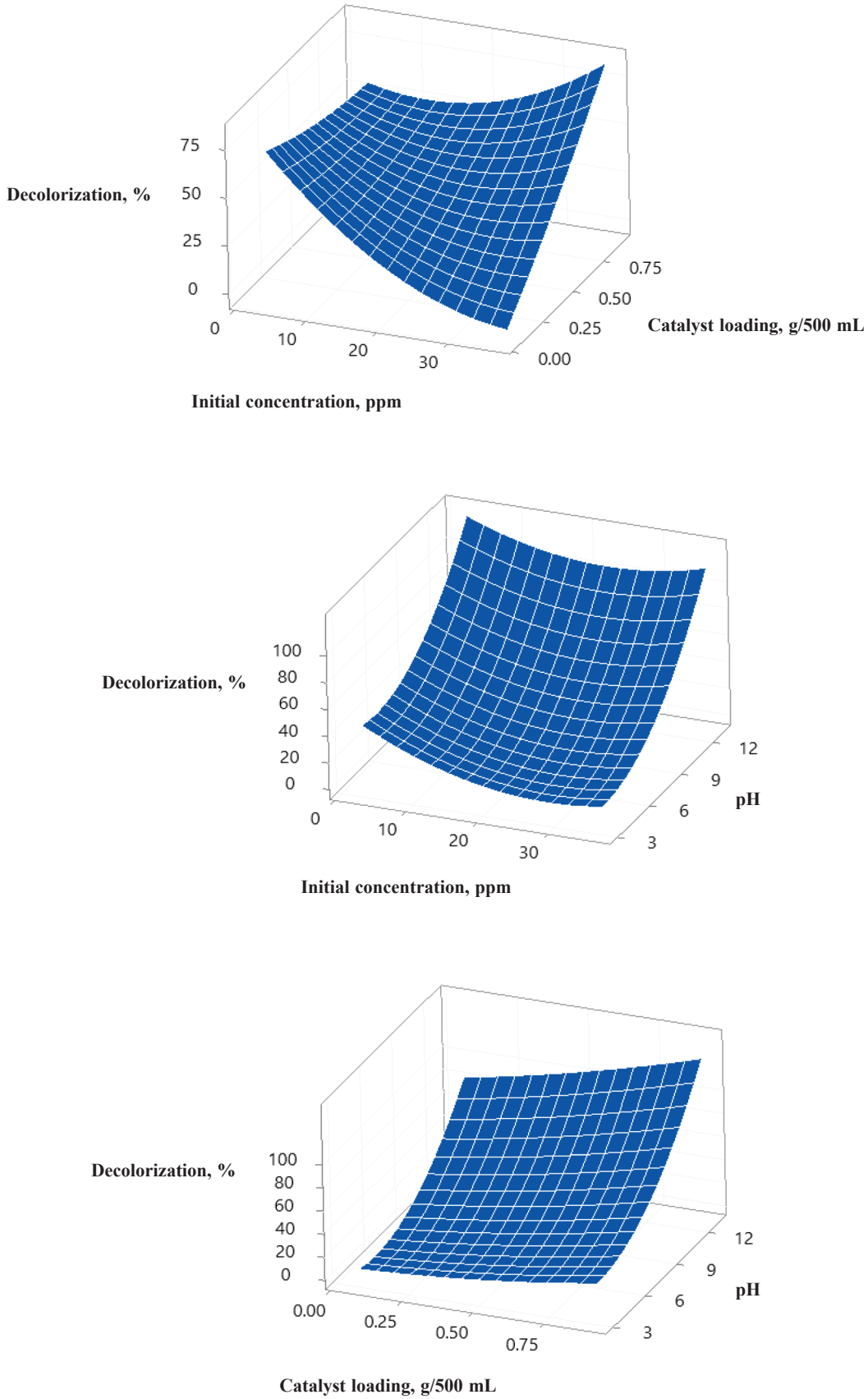

F i g . 6 – *Surface plots of: decolorization % vs catalyst loading, initial concentration (a), decolorization % vs pH, initial concentration (b), and decolorization % vs pH, catalyst loading (c)*

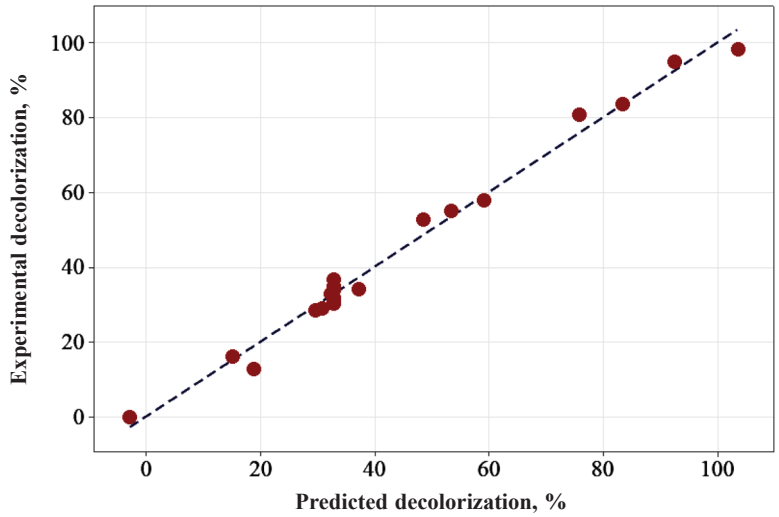

Fig. 7 – *Actual (experimental) vs. predicted values for decolorization of Rh 6G*

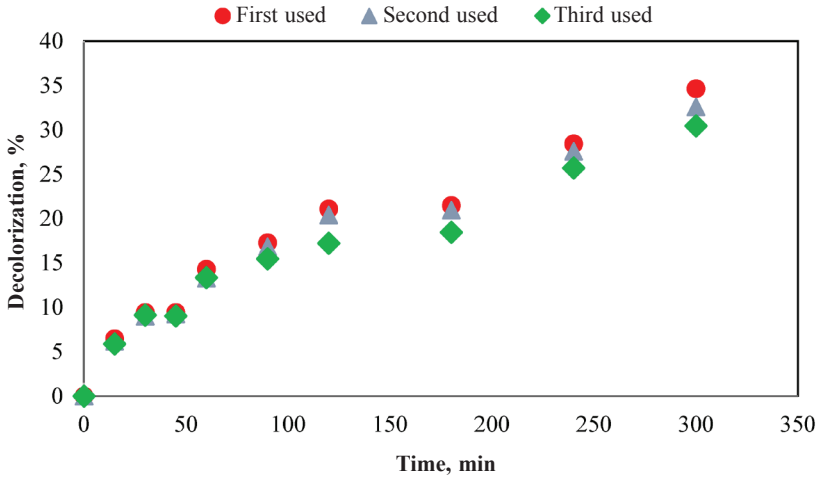

Fig. 8 – *Stability of TiO_2@Fe_3O_4/FeZSM-5 catalyst*

water, treated, and untreated wastewaters. From the root length the inhibition percentage was calculated for the treated and untreated wastewaters using the formula given below:

$$\text{Inhibition, \%} = \frac{\text{Root Length}_{\text{distilled water}} - \text{Root Length}_{\text{sample}}}{\text{Root Length}_{\text{distilled water}}} \quad (3)$$

The inhibition values were 65.04 % and 17.86 % for the untreated and treated Rh 6G solutions, respectively. The decrease in inhibition value indicates the reduction in toxicity.

Comparison with other studies

In literature there are some studies on photocatalytic oxidation of various organic pollutants over magnetic photocatalysts. Yang *et al.*[22] studied the photocatalytic oxidation of methylene blue over Fe_3O_4@rGO@TiO_2 in the presence of H_2O_2 under xenon lamp irradiation, and they achieved almost complete degradation in 120 min. Similarly, TiO_2-Fe_3O_4-bentonite was used efficiently as magnetic photocatalyst for degradation of methylene blue under xenon lamp irradiation.[29] Chang *et al.*[44] and Razip *et al.*[3] synthesized Fe_3O_4/TiO_2 photocatalyst for photocatalytic oxidation of phenol and methyl orange, respectively, under UV-C light irradiation. A degradation of methyl orange of 90.3 % and almost complete degradation of phenol was achieved within 150 min, respectively. In another study, UV-A was used as a light source for antibiotics removal over Fe_3O_4/ZnO photocatalyst.[45] However, xenon lamps are difficult to install, expensive, and short-lived. As well known, ultraviolet light (λ = 254 nm) occupies only 4– 5 % of the solar spectrum. In the present study, high-pressure Na lamps, which are inexpensive, environmentally friendly, and easy to install, were used as a light source, and almost complete decolorization was achieved at optimum conditions.

Conclusions

The photocatalytic oxidation of Rh 6G dye was investigated over TiO_2@Fe_3O_4/FeZSM-5 magnetically separable photocatalyst. Effect of operating parameters on decolorization of Rh 6G was evaluated by the Central Composite Design with surface and interaction plots. Maximum photocatalytic decolorization percentage of 98.2 % was found at optimum conditions of 20 mg L^{-1} Rh 6G, 1 g L^{-1} of catalyst, and alkaline pH of 13.04. Analysis of variance (ANOVA) showed a high lack-of-fit value of 0.08 that indicated satisfactory agreement of the second-order regression model with the experimental data. For toxicity test, inhibition was measured as 65.04 % and 17.86 % for the untreated and treated Rh 6G solutions, respectively. In addition to color removal, the toxicity of the Rh 6G aqueous solution was significantly reduced by photocatalytic oxidation over TiO_2@Fe_3O_4/FeZSM-5 photocatalyst. Due to the magnetic property of the catalyst, the sample could be removed from dye solution easily with the help of magnetic field. Therefore, the TiO_2@Fe_3O_4/FeZSM-5 photocatalyst showed not only photocatalytic activity performance for decolorization of Rh 6G dye under visible light irradiation, but also excellent recycling/separability properties, which is of great importance if it is desired to be used in large-scale applications.

Supplementary Materials

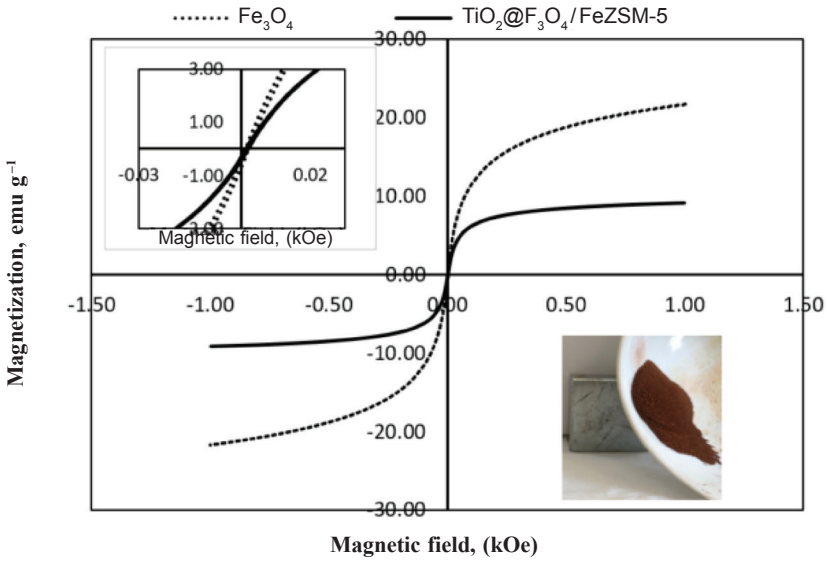

Fig. 1*S – VSM analysis of prepared catalysts*

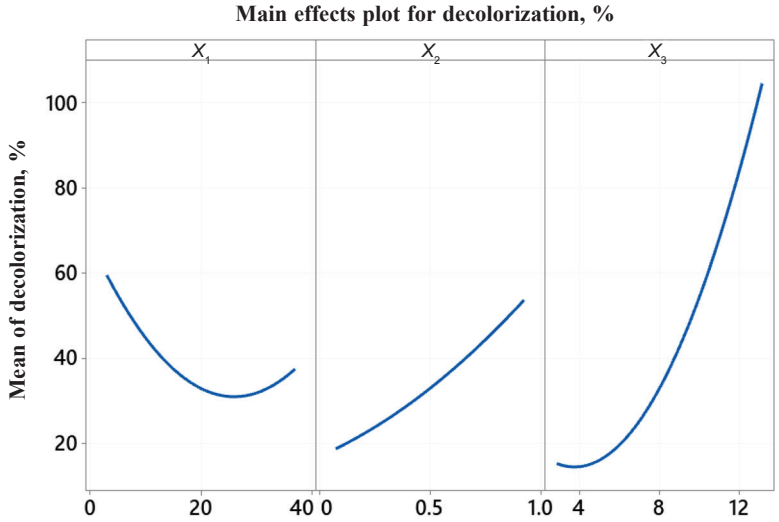

Fig. 2*S – Main effect plot of decolorization of Rh 6G (X_1: Initial concentration, X_2: Catalyst loading, X_3: pH)*

ACKNOWLEDGEMENT

The author acknowledges the financial support from Ege University Scientific Research Fund under Project No. 18MÜH026. The author also acknowledges the assistance and guidance of Professor Gönül Gündüz during this study.

References

1. *Roge, V., Guignard, C., Lamblin, G., Laporte, F., Fechete, I., Garin, F., Dinia, A., Lenoble, D.*, Photocatalytic degradation behavior of multiple xenobiotics using MOCVD synthesized ZnO nanowires, Catal. Today **306** (2018) 215. doi: https://doi.org/10.1016/j.cattod.2017.05.088
2. *Rajoriy, S., Bargole, S., Saharan, V. K.*, Degradation of a cationic dye (Rhodamine 6G) using hydrodynamic cavitation coupled with other oxidative agents: Reaction mechanism and pahway, Ultrason. Sonochem. **34** (2017) 183. doi: https://doi.org/10.1016/j.ultsonch.2016.05.028
3. *Razip, N. I. M., Lee, K. M., Lai, C. W., Ong, B. H.,* Recoverability of Fe_3O_4/TiO_2 nanocatalyst in methyl orange degradation, Mater. Res. Express **6** (2019) 1. doi: https://doi.org/10.1088/2053-1591/ab176e
4. *Wawrzkiewicz, M., Hubicki, Z.,* Anion exchange resins as effective sorbents for removal of acid, reactive, and direct dyes from textile wastewaters, IntechOpen, Ion Exchange – Studies and Applications, (2015) Chapter 2. doi: https://doi.org/10.5772/60952
5. *Gao, L., Zhang, Q., Li, J., Feng, R., Xu, H., Xue, C.*, Adsorption of Methyl orange on magnetically separable mesoporous titania nanocomposites, Chin. J. Chem. Eng. **22** (2014) 1168. doi: https://doi.org/10.1016/j.cjche.2014.09.015
6. *Babaei, A. A., Alavi, S. N., Akbarifar, M., Ahmadi, K., Esfahani, A. R., Kakavandi, B.,* Experimental and modeling study on adsorption of cationic methylene blue dye onto mesoporous biochars prepared from agrowaste, Desalin. Water Treat. **57** (2016) 1. https://doi.org/10.1080/19443994.2016.1163736
7. *Kermani, M., Izanloo, H., Kalantary, R. R., Barzaki, H. S., Kakavandi, B.*, Study of the performances of low cost adsorbents extracted from *Rosa damascena* in aqueous solutions decolorization, Desalin. Water Treat. **80** (2017) 357. doi: https://doi.org/10.5004/dwt.2017.21019
8. *Azari, A., Gholami, M., Torkshavand, Z., Yari, A. R., Ahmadi, E., Kakavandi, B.,* Evaluation of Basic Violet 16 adsorption from aqueous solution by magnetic zero valent iron-activated carbon nanocomposite using response surface method: Isotherm and kinetic studies, J. Mazandaran Univ. Med. Sci. **25** (2015) 333.
9. *Dewi, S. H., Fisli, A., Wardiyati, S.*, Synthesis and characterization of magnetized photocatalyst $Fe_3O_4/SiO_2/TiO_2$ by heteroagglomeration method J. Phys.: Conf. Ser. **739** (2016) 1. doi: https://doi.org/10.1088/1742-6596/739/1/012113
10. *Dükkancı, M.*, A parametric study on the heterogeneous photo-fenton-like oxidation of bisphenol-a over an Fe/TiO_2 catalyst under visible light, J. Polytech. **20** (2017) 25. doi: https://doi.org/10.2339/2017.20.1
11. *Shojaei, A. F., Shams-Nateri, A.*, Magnetically recyclable $Fe^{3+}/TiO_2@Fe_3O_4$ nanocomposites towards degradation of direct blue 71 under visible-light irradiation, Micro Nano Lett. **12** (2017) 161. doi: https://doi.org/10.1049/mnl.2016.0620
12. *Salamat, S., Younesi, H., Bahramifar, N.*, Synthesis of magnetic core-shell $Fe_3O_4@TiO_2$ nanoparticles from electric arc furnace dust for photocatalytic degradation of steel mill wastewater, RSC Adv. **7** (2017) 19391. doi: https://doi.org/10.1039/c7ra01238a
13. *Babaei, A. A., Golshan, M., Kakavandi, B.*, A heterogeneous photocatalytic sulfate radical-based oxidation process for efficient degradation of 4-chlorophenol using TiO_2 anchored on Fe oxides@carbon, Process Saf. Environ. **149** (2021) 35. doi: https://doi.org/10.1016/j.psep.2020.10.028
14. *Rezai, S. S., Kakavandi, B., Noorisepehr, M., Isari, A. A., Zabih, S., Bashardoust, P.*, Photocatalytic oxidation of tetracycline by magnetic carbon-supported TiO_2 nanoparticles catalyzed peroxydisulfate: Performance, synergy, and reaction mechanism studies, Sep. Purif. Technol. **258** (2021) 117936. doi: https://doi.org/10.1016/j.seppur.2020.117936
15. *Bashiri, F., Khezri, S. M., Kalantary, R. R., Kakavandi, B.*, Enhanced photocatalytic degradation of metronidazole by TiO_2 decorated on magnetic reduced graphene oxide: Characterization, optimization and reaction mechanism studies. J. Mol. Liq. **314** (2020) 113608. doi: https://doi.org/10.1016/j.molliq.2020.113608
16. *Xin, T., Ma, M., Zhang, H., Gu, J., Wang, S.,* A facile approach for the synthesis of magnetic separable $Fe_3O_4@TiO_2$, core-shell nanocomposites as highly recyclable photocatalysts, Appl. Surf. Sci. **288** (2014) 51. doi: https://doi.org/10.1016/j.apsusc.2013.09.108
17. *Yeh, N., Lee, Y. C., Chang, C. Y., Cheng, T. C.*, Anti-fish bacterial pathogen effect of visible light responsive $Fe_3O_4@TiO_2$ nanoparticles immobilized on glass using TiO_2 sol-gel, Thin Solid Films **549** (2013) 93. doi: https://doi.org/10.1016/t.tsf.2013.09.092
18. *Villa, S., Caratto, V., Locardi, F., Alberti, S., Sturini, M., Speltini, A., Maraschi, F., Canepa, F., Ferretti, M.*, Enhancement of TiO_2 NPs activity by Fe_3O_4 nano-seeds for removal of organic pollutants in water, Materials **9** (2016) 1. doi: https://doi.org/10.3390/ma9090771
19. *Behrad, F., Farimani, M. H. R., Shahtahmasebi, N., Roknabadi, M. R., Karimipour, M.,* Synthesis and characterization of Fe_3O_4/TiO_2 magnetic and photocatalyst bifunctional core-shell with superparamagnetic performance, Eur. Phys. J. Plus **130** (2015) 1. doi: https://doi.org/10.1140/epjp/i2015-15144-y
20. *Stefan, M., Pana, O., Leostean, C., Bele, C., Silipas, D., Senila, M., Gautron, E.*, Synthesis and characterization of Fe_3O_4-TiO_2 core-shell nanoparticles, J. Appl. Phys. **116** (2014) 1. doi: https://doi.org/10.1063/1.4896070
21. *Lin, Y., Geng, Z., Cai, H., Ma, L., Chen, J., Zeng, J., Pan, N., Wang, X.*, Ternary graphene-TiO_2-Fe_3O_4 nanocomposite as a recollectable photocatalyst with enhanced durability, Eur. J. Inorg. Chem. **2012** (2012) 4439. doi: https://doi.org/10.1002/ejc.201200454
22. *Yang, X., Chen, W., Huang, J., Zhou, Y., Zhu, Y., Li, C.,* Rapid degradation of methylene blue in a novel heterogeneous $Fe_3O_4@rGo@TiO_2$-catalyzed photo-Fenton system, Sci. Rep. **5** (2015) 1. doi: https://doi.org/10.1038/srep10632
23. *Wei, X. N., Wang, H. L.*, Preparation of magnetic g-C_3N_4/Fe_3O_4/TiO_2 photocatalyst for visible light photocatalytic application, J. Alloys Compd. **763** (2018) 844. doi: https://doi.org/10.1016/j.jallcom.2018.06.031
24. *Dong, Q., Zhang, K., An. Y.*, A novel synthesis method for TiO_2 particles with magnetic Fe_3O_4 cores, Water Sci. Technol. **69** (2014) 2093. doi: https://doi.org/10.2166/wst.2014.121

25. *Benjwal, P., Kumar, M., Chamoli, P., Kar, K. K.*, Enhanced photocatalytic degradation of methylene blue and adsorption of arsenic (III) by reduced graphene oxide (rGO)-metal oxide (TiO_2/Fe_3O_4) based nanocomposites, RSC. Adv. **5** (2015) 73249.
doi: https://doi.org/10.1039/c5ra13689j
26. *Taufik, A., Saleh, R.*, Combination of ternary Fe_3O_4/TiO_2/CuO nanocomposites and nanographene platelets: High performance photo and sonocatalysis, Int. Conf. Eng., Sci. Nanotechnol., AIP Conf. Proc., Indonesia **1788** (2017) 030037, 1.
doi: https://doi.org/10.1063/1.4968290
27. *Wang, R., Wang, X., Xi, X., Hu, R., Jiang, G.*, Preparation and photocatalytic activity of magnetic Fe_3O_4/SiO_2/TiO_2 composites, Adv. Mater. Sci. Eng. **409379** (2012) 1.
doi: https://doi.org/10.1155/2012/409379
28. *Kalan, R. E., Yaparatne, S., Amirbahman, A., Tripp, C. P.*, P25 titanium dioxide coated magnetic particles: Preparation, characterization and photocatalytic activity, Appl. Catal. B **187** (2016) 249.
doi: https://doi.org/10.1016/j.apcatb.2016.01.008
29. *Chen, W., Xiao, H., Xu, H., Ding, T., Gu, Y.*, Photodegradation of methylene blue by TiO_2-Fe_3O_4-bentonite magnetic nanocomposite, Int. J. Photoenergy **591428** (2015) 1. https://doi.org/10.1155/2015/591428
30. *Dükkancı, M.,* Magnetically recyclable Fe_3O_4@TiO_2 composites in photocatalytic degradation of Rhodamine 6G dye under visible-light irradiation, Int. Symp. Compos. Mater., [Proc.], 4th, KompEGE 2018 Proceeding book, Turkey (2018) 474.
31. *Dükkancı, M., Vinatoru, M., Mason, T. J.*, The sonochemical decolourisation of textile azo dye orange II: Effects of Fenton type reagents and UV light, Ultrason. Sonochem. **21** (2014) 846.
doi: https://doi.org/10.1016/j.ultsonch.2013.08.020
32. *Hörmann, U., Kaiser, U., Albrecht, M., Geserick, J., Hüsing, N.,* Structure and luminescence of sol-gel synthesized anatase Nanoparticles, 16th Int. Conf. Microsc. Semicond. Mater., J. Physics: Conf. Ser. 012039, **209** (2010) 1.
doi: https://doi.org/10.1088/1742-6596/209/1/012039
33. *Mi, M. L., Johnsen, S., Clausen, C., Hald, P., Lock, N., So, L., Iversen, B. B.*, Highly controlled crystallite size and crystallinity of pure and iron-doped anatase-TiO_2 nanocrystals by continuous flow supercritical synthesis, J. Mater. Res. **28** (2013) 333.
doi: https://doi.org/10.1557/jmr.2012.234
34. *Yan, H., Wang, X., Yao, M., Yao, X.*, Band structure design of semiconductors for enhanced photocatalytic activity: The case of TiO_2, Prog. Nat. Sci. Mater. **23** (2013) 402.
35. *Khataee, A. R., Fathinia, M., Aber, S., Zarei, M.,* Optimization of photocatalytic treatment of dye solution on supported TiO_2 nanoparticles by central composite design: Intermediates identification, J. Hazard. Mater. **181** (2010) 886.
doi: https://doi.org/10.1016/j.jhazmat.2010.05.096
36. *Lee, K. M., Hamid, S. B. A.*, Simple Response Surface methodology: Investigation on advance photocatalytic oxidation of 4-chlorophenoxyacetic acid using UV-active ZnO photocatalyst, Materials **8** (2015) 339.
doi: https://doi.org/10.3390/ma8010339
37. *Shafaei, A., Nikazar, A., Arami, M.*, Photocatalytic degradation of terephthalic acid using titania and zinc oxide photocatalysts: Comparative study, Desalination **252** (2010) 8.
doi: https://doi.org/10.1016/j.desal.2009.11.008
38. *Mosleh, S., Rahimi, M. R., Ghaedi, M., Dashtian, K.,* Sonophotocatalytic degradation of trypan blue and vesuvine dyes in the presence of blue light active photocatalyst of Ag_3PO_4/Bi_2S_3-HKUST-1-MOF: Central composite optimization and synergistic effect study, Ultrason. Sonochem. **32** (2016) 387.
doi: https://doi.org/10.1016/j.ultsonch.2016.04.007
39. *Muthukumar, M., Sargunamani, D., Selvakumar, N., Rao, J. V.*, Optimization of ozone treatment for colour and COD removal of acid dye effluent using central composite design experiment, Dyes Pigm. **63** (2004) 127.
doi: https://doi.org/10.1016/j.dyepig.2004.02.003
40. *Gomri, F., Finqueneisel, G., Zimny, T., Korili, S. A., Gil, A., Boutahala, M.*, Adsorption of Rhodamine 6G and humic acids on composite bentonite–alginate in single and binary systems, Appl. Water Sci. **8** (2018) 156.
doi: https://doi.org/10.1007/s13201-018-0823-6
41. *Arambasic, M. B., Bjelic, S., Subakov, G.,* Acute toxicity of heavy metals (copper, lead, zinc), phenol and sodium on *Allium cepa* L., *Lepedium stavum* L. and *Daphnia magna* St.: Comparative investigations and the practical applications, Water Res. **29** (1995) 497.
doi: https://doi.org/10.1016/0043-1354(94)00178-A
42. *Demir, N., Gündüz, G., Dükkancı, M.,* Degradation of a textile dye, Rhodamine 6G (Rh 6G), by heterogeneous sonophoto-Fenton process in the presence of Fe containing TiO_2 catalysts, Environ. Sci. Pollut. R. **22** (2015) 3193.
doi: https://doi.org/10.1007/s11356-014-2868-x
43. *Dükkancı, D.,* Treatment of Bisphenol-A using sonication-assisted photo-Fenton hybrid process: Influence of reaction parameters, Chem. Biochem. Eng. Q. **33** (2019) 43.
doi: https://doi.org/10.15255/CABEQ.2018.1487
44. *Chang, J., Zhang, Q., Liu, Y., Shi, Y., Qin, Z.*, Preparation of Fe_3O_4/TiO_2 magnetic photocatalyst for photocatalytic degradation of phenol, J. Mater. Sci.: Mater. Electron. **29** (2018) 8258.
doi: https://doi.org/10.1007/s10854-018-8832-7
45. *Fernandez, L., Gamallo, M., Gonzalez-Gomez, Vaques-Vazques, C., Rivas, J.,* Insight into antibiotics removal: Exploring the photocatalytic performance of a Fe_3O_4/ZnO nanocomposite in a novel magnetic sequential batch reactor, J. Environ. Manage. **237** (2019) 595.
doi: https://doi.org/10.1016/j.jenvman.2019.02.089